

11-5  
Analog Analyses of Seismograms Recorded on Magnetic Tape<sup>1</sup>

GEORGE H. SUTTON AND PAUL W. POMEROY

Lamont Geological Observatory, Columbia University  
Palisades, New YorkNASw-82  
N63 17909

Code none

**Abstract.** Routine recording of long-period seismometer signals in analog form on magnetic tape makes it possible to perform a wide variety of analyses rapidly and efficiently. Examples of analog analyses of seismic waves from eight distant earthquakes, a large nuclear explosion, and the microseism storm associated with a hurricane illustrate some of the advantages of this type of recording. Inverse and selective filtering, with and without filter phase shift, are used to remove instrumental effects, improve signal-to-noise ratio, and emphasize desired phases. Fourier, energy, and power spectrums are obtained by several analog methods. Comparison of results of an analog Fourier analysis of the Palisades record of a large Soviet nuclear explosion near Novaya Zemlya in 1961 with digital analyses of two smaller 1958 explosions in the same area recorded at Palisades shows remarkable similarity in the spectrums. The only significant difference between the two sets of data is that the larger event is richer in long-period energy. Plots of frequency versus time and of cumulative signal, in different frequency bands, versus time present seismic data in a form more convenient for certain studies than the conventional record. Various combinations of the original three-component signals (N-S, E-W, and vertical) permit easy identification of seismic wave types by surface particle motion, improve the precision and reliability with which seismic arrivals can be identified, and aid in the detailed study of near-station effects on seismic signals. Results from the rotation of apparent instrumental coordinates to longitudinal horizontal, transverse horizontal, and vertical; multiplication of vertical and longitudinal components; and integration of this product serve as examples of the advantages of this type of data transformation. The analog magnetic tape seismograms can be digitized for any digital analyses desired, using a relatively simple, automatic, low-speed digitizer (two 3-decimal digit readings per second).

## INTRODUCTION

The routine recording of long-period seismic signals in analog form on magnetic tape allows a wide variety of analyses to be performed in a rapid and efficient manner. Because of the ease of handling data recorded on magnetic tape, long time intervals and/or large numbers of events can be handled on a routine basis. Many

advantages of recording on magnetic tape have been known for some time and, in fact, have been extensively utilized in other areas. Wide-band field recordings on magnetic tape have been made for several years in seismic exploration, generally in the frequency range above 1 cps. For this application, narrow-band filtering and other techniques are used during subsequent analysis in the laboratory; however, the original data and the objectives of the analysis are quite different from those discussed in this paper.

Benioff and Gutenberg [1952] recorded sev-

eral earthquakes, including the long-period surface waves, by amplitude modulation on magnetic tape running at slow speed. Ewing *et al.* [1959, 1961b] used a copy of Benioff's records to study dispersion in the surface and body waves from explosions and earthquakes with a vibration analyzer. Carey, in Tasmania, is recording short-period seismic signals on slow-speed magnetic tape recorders, as reported by Newstead and Watt [1960].

Bogert [1961b] recorded seismic signals on magnetic tape and converted the data to digital form before analysis. Willmore [1960] suggested that the use of recording mediums such as magnetic tape might be the next large step forward in seismic data analysis. Investigators in Japan [Omote *et al.*, 1955; Omote and Yamazaki, 1957] have also recorded short-period seismic signals on magnetic tape.

Other investigators are developing direct digital recording of seismic signals on paper tape or cards or magnetic tape [Haubrich and Iyer, 1962; DeBremacker *et al.*, 1962; Miller, 1963;

<sup>1</sup> Lamont Geological Observatory Contribution 615.

Hagelbarger, 1961; Simpson, 1961]. The advantages of the wide dynamic range of these recording systems are somewhat offset by the time required for data reduction and analysis, the amount of recording medium needed, and the requirement for a digital computer for even the most elementary analysis. An implicit requirement for such systems is that the primary transducer and any preamplifiers have an equally wide dynamic range.

The purpose of the present paper is to describe the magnetic tape recording system currently in operation at the Lamont Geological Observatory and to present some methods and preliminary results of the reduction and analysis of seismic signals recorded with this system. These include (1) inverse filtering to remove instrumental effects, and selective filtering to emphasize various phases, including filtering without phase shift; (2) plotting of frequency versus time and cumulative energy versus time; (3) determination of Fourier, energy, and power spectrums; (4) rotation of instrumental axes; (5) identification, by surface particle motion, of seismic wave types; and (6) analog-to-digital conversion. Future plans include the purchase of higher-speed analog-to-digital conversion equipment for subsequent digital analysis.

The Lamont Observatory is establishing a worldwide network of long-period, magnetic tape recording stations which are producing data to be handled by these methods. Also, seismic data from the Ranger and subsequent experiments on the moon can be analyzed using as many of the above techniques as are applicable. Barometric, gravimetric, and magnetic observations are currently being recorded on magnetic tape and are being, or will be, analyzed with the same equipment. Magnetic tape records from ocean bottom seismographs and other short-period field instruments are also being analyzed at this facility.

#### INSTRUMENTATION

*Recording equipment.* Present instrumentation consists of the following components:

(a) *Seismometers.* The long-period (three components) seismometers are of the Columbia type with a 500-ohm transducer coil. The operating period of these instruments is currently 15 seconds. Some records were obtained with the instruments operating at 30 seconds. Short-period Benioff portable seismometers (three com-

ponents with natural periods of 1 second) are also being recorded routinely.

(b) *Preamplifiers.* Since the power available from a seismometer transducer coil is very small, preamplifiers are required. The preamplifiers should be stable, low-level amplifiers. If long-period prefiltering is desired, a relatively high input impedance is required. The amplifier (dc) currently in use is the Honeywell deviation amplifier, which is down in response by 3 db at 4 cps. Other amplifiers, including the Hewlett-Packard 425-A, have been used in the past.

(c) *Filters.* At the present time, simple long-period low-pass RC filters are being used. These filters are sometimes combined with additional shorter-period low-pass or band-rejection filters. The unfiltered seismometer coil output is also recorded.

(d) *Recorders.* The amplified and prefiltered seismometer output is divided into high- and low-gain levels and recorded as a frequency-modulated signal on  $\frac{1}{2}$ -inch magnetic tape.<sup>2</sup> Both Ampex and Honeywell tape systems are being used. Present recording speeds are 15/16 ips, which provides a 24-hour record on a 14-inch reel of instrumentation grade tape having a 1-mil base, and 0.06 ips, which provides a 16-day record on a similar tape reel. Signal-to-noise ratio for the Ampex system is about 40 db in the signal passband after re-recording once. For the Honeywell system, the signal-to-noise ratio is about 50 db in the signal passband. Visible monitor records are obtained in parallel with the magnetic tape records. Drum-mounted potentiometer recorders (Varian Instrument Company, G-10) are used to monitor the long-period instruments, and Geotechnical Corporation Helicorders are used for the short-period instruments. These units provide a permanent visible record of the input to the tape recorders. Although monitoring of the tape output would be preferable for reliability, practical considerations preclude this possibility at present.

For economic and practical reasons, storage of the magnetic tape at a rate of one reel per day

<sup>2</sup> The tape transports have 7 recording channels (IRIG configuration). The long- and short-period signals are recorded on separate transports. For the long-period system, the seventh channel is used for timing. For the short-period system the seventh channel is used for compensation, and time marks are superimposed on a low-gain data channel.

CASE FILE COPY

is not feasible; therefore, the recordings from the higher-speed tape system are compressed in length by a factor of 32 before storage, and up to one month's records can be stored on a single reel. The compression in length is accomplished by speeding up the data by the proper amount and recording on another magnetic tape unit operating at a lower tape speed. For the Ampex system, with a compression in length of 32, the bandwidth, referred to the original data, is 0 to 5 cps. For the Honeywell system, the data bandwidth is 0 to 20 cps. Thus, for both systems, the system response is limited by the preamplifier response to 0 to 4 cps.

The time compression factor (frequency increase) is obtained by multiplying the compression in length on the storage reel by the ratio of the final reproducing speed to the original recording speed. For special analysis, the data can be re-expanded or further compressed without an objectionable loss of signal quality. Time compression allows the use of audio and sub-audio frequency analyzing equipment for the long-period data and reduces the time required for many types of analyses. In addition, by expanding the time scale, high-frequency signals can be studied in detail and digitized with relatively inexpensive, slow-speed equipment.

*Analyzing equipment.* A flow chart of the existing data analysis facility at Lamont Observatory is shown in Figure 1. The magnetic tape seismogram is reproduced at the desired speed on a standard tape transport in positive or negative record time. The resulting signal can be analyzed directly, digitized for subsequent digital analysis, or re-recorded on a magnetic tape loop transport for subsequent analog analysis requiring data repetition.

(a) Filters. Krohn-Hite 330A-4 variable band-pass or low-pass filters with a frequency range of 0.005 to 500 cps are currently in use. These have a minimum passband of 1 octave between 3-db points and an attenuation slope of 24 db/octave. An Allison model 201 variable band-pass, high-pass, or low-pass filter using passive components is also available. This filter has a frequency range of 1 to 256 cps, minimum passband of 1/5 octave, and an attenuation slope of 30 db/octave. A Krohn-Hite 350A variable band-rejection filter with a frequency range of 0.02 to 2000 cps is also used. For routine operations, fixed filters such as inverse seismographs or notch filters for rejection of microseisms can be constructed using analog computer components.

(b) General purpose analog computer. A

### LAMONT GEOLOGICAL OBSERVATORY DATA ANALYSIS FACILITY

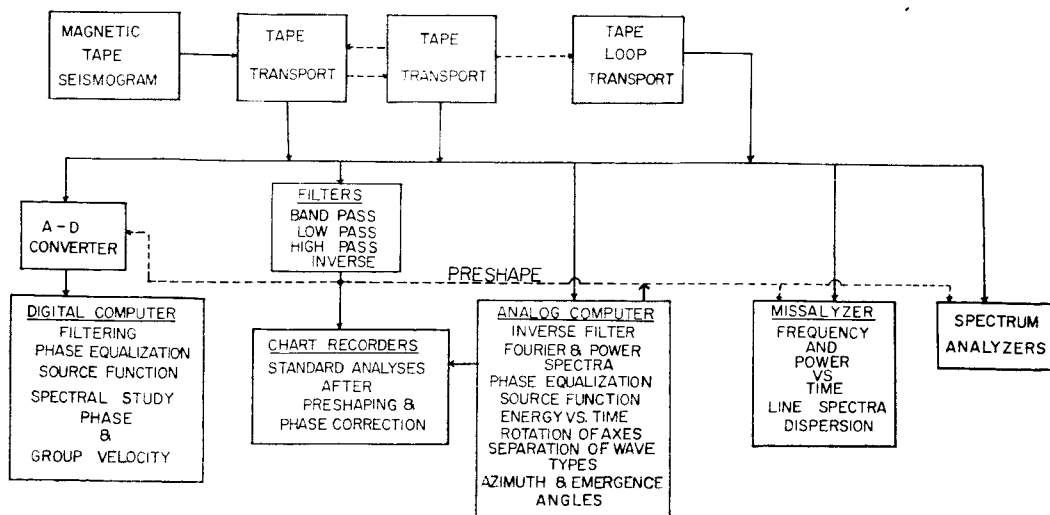


Fig. 1. Flow chart of data analysis facility.

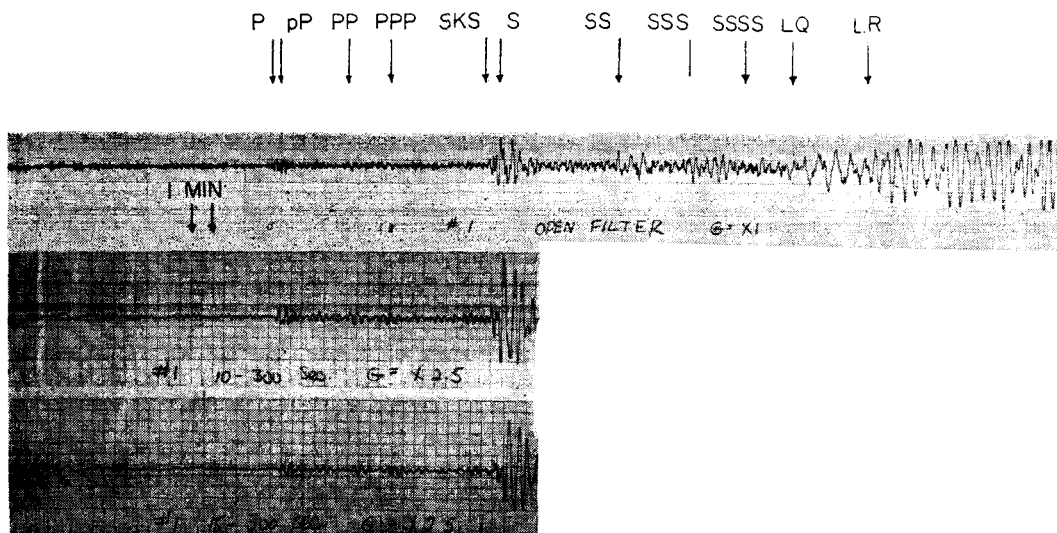


Fig. 2. N-S seismograms of Kurile Islands earthquake. *Upper*, open filter; *middle*, 10-sec low-pass filter; *lower*, 15-sec low-pass filter. Body wave arrival times shown in this and succeeding figures are from Jeffreys-Bullen tables. Epicentral data for this and other events studied are given in Table 1.

Pace TR-10 (Electronic Associates, Inc.) analog computer with twenty operational amplifiers, ten integrators and multipliers, and other nonlinear devices is being used.

(c) Frequency analyzers. Two types of standard analyzers are currently in use. The Misislyzer, manufactured by Kay Electric Co., provides measurements of frequency and amplitude envelope versus time, and amplitude versus frequency for selected small time intervals. A spectrum analyzer manufactured by Technical Products Corporation is used to produce spectrums from complete seismograms.

(d) Chart recorders. Sanborn chart recorders are generally used for presentation of the analyzed data.

(e) Analog-to-digital converter. A Datex shaft position encoder is mounted on a Varian recorder so that an incoming signal may be digitized directly or a signal on magnetic tape may be converted to digital format. This unit operates into a paper card punch (IBM 026) or a paper tape punch (Friden SP-2) at a maximum rate of two 3-digit conversions per second.

In addition, a drum-mounted shaft-position encoder is available for digitizing standard seismograms. This unit can also be used to provide an electrical analog for magnetic tape recording from a standard seismogram.

## METHODS AND RESULTS

*Selective filtering.* One of the advantages possessed by magnetic tape recording is that it allows the repeated reproduction of the recorded signal, with the result that the signal may be studied in several different ways. The signal may be reproduced wide-band, that is, with no filters between the tape output and the visible recorder. Then, low-pass, high-pass, band-pass, or band-rejection filters may be used to emphasize or attenuate selected portions of the frequency spectrum. In many cases, filtering without introducing phase shift is desirable, and this is possible with analog techniques. The effect of instrumental response may be removed from the recorded seismogram and/or the response may be shaped to any reasonable characteristic by means of inverse filtering.

A set of records which is particularly valuable for studies of the longer-period components can be obtained by setting the filter at wide-band and then successively lowering the low-pass corner. Figure 2 shows records of the N-S long-period signal from the Kurile Islands earthquake of September 3, 1960, recorded at Palisades. The source data for this earthquake and all other events discussed in this paper are listed in Table 1.

The seismometer has a free period of 30 sec-

onds, and the signal is prefiltered with a two-stage passive RC low-pass filter, set at 45 seconds corner period (equivalent to a critically damped galvanometer with a natural period of 45 seconds), before recording on magnetic tape. The time base is compressed during playback by a factor of 32; thus a half-hour record is analyzed in a minute. The records shown are obtained by reproducing the recorded signal through a band-pass filter. In the top trace, the filter was effectively open (signal periods of 1 to 300 seconds in real time). The two lower traces show the effect of low-pass filtering at 10 to 300 and 15 to 300 seconds, respectively. On these lower traces, the predominant microseism noise in the period range of 4 to 8 seconds has been strongly attenuated relative to the body waves. The signal-to-noise ratio for the *P* wave, for ex-

ample, has been increased by about a factor of 3. Since the *P* wave spectrum is broader than that of the microseisms, the signal-to-noise ratio could also be improved by high-pass (or band-rejection) filtering.

Shown in Figure 3 is a series of N-S records recorded on tape at Palisades from the Dominican Republic earthquake of September 14, 1960. From top to bottom, the low-pass filter setting is successively increased from 1 to 48 seconds. The following improvements can be noted in the records: first, the microseisms are attenuated by the filtering process; second, the pulselike character of *P* and *PP* is emphasized by the successive filtering; third, the beginning of the Rayleigh wave, which is obscured by earlier arrivals in the wider-band traces, is clearly seen on the 32- to 300-second filtered trace.

TABLE 1. Epicentral Data and Distance and Azimuth at Palisades, New York, for the Earthquakes and the Explosion Used in This Study

Date	Location*	Origin Time,*			Depth,* km	Magnitude	Distance, deg	Azimuth, deg
		h	m	s				
1960								
Sept. 3	44.6°N, 149.1°E Kurile Islands	23	46	23.9	27	6¼ (Pas)	86.2	330.8
Sept. 14	35.1°S, 106.0°W South Pacific Ocean	04	57	12.5	40	not given	81.3	206.2
Sept. 14	19.6°N, 70.3°W Dominican Republic	01	53	32.1	103	not given	21.6	170.2
1961								
June 16	8.8°N, 73.4°W Northern Colombia	10	31	56.2	120	6 (Pas)	32.1	179.1
Oct. 30	74.7°N, 54.9°E Novaya Zemlya	08	33	30	<0	5¼-5½ (Pal)	59.7	13.9
Dec. 20	4.6°N, 75.6°W West-central Colombia	13	25	34.4	176	6-¾ (Pas) 6 (Pal)	36.3	182.9
Dec. 30	52.3°N, 177.7°E Rat Islands, Aleutian Islands	00	39	24.1	52	7 (Pal) 6¾ (Pas) 6½ (Berk)	68.3	321.2
1962								
Feb. 14	38.1°S, 73.1°W Near Coast of Chile	06	36	01.3	44	6¾-7 (Pal) 7¼ (Pas) 7½ (Berk)	78.6	179.4
Sept. 1	35.6°N, 50.0°E Northwest Iran	19	20	38.5	21	7 (Pal) 7¼ (Pas) 7¾ (Berk)	88.0	42.6

\* Determined by U. S. Coast and Geodetic Survey except for October 30, 1961, event for which coordinates and origin times are taken from the Uppsala, Sweden, Seismological Bulletin.

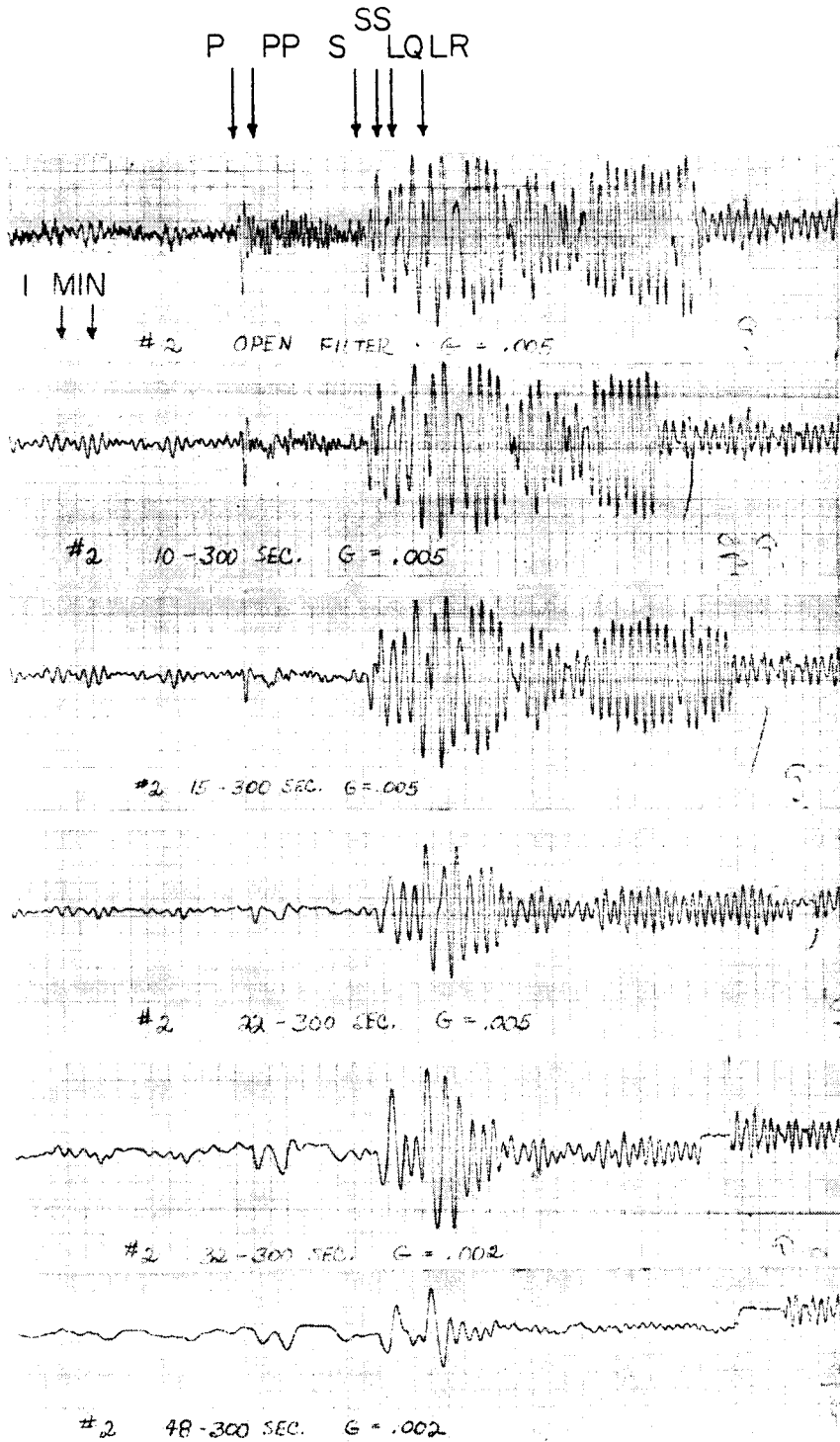


Fig. 3. N-S seismograms of Dominican Republic earthquake. Low-pass filter corners, open, 10, 15, 22, 32, and 48 seconds, from top to bottom.

Figure 4 shows playbacks of Palisades N-S magnetic tape seismograms from the South Pacific earthquake of September 14, 1960. As the low-pass filter setting is moved to successively longer periods, the storm microseisms in the 6-second period range are effectively removed and the signal-to-noise ratio is generally improved. On the lower traces, there is apparent inverse dispersion in the shear and Rayleigh

wave trains. This apparent inverse dispersion will be discussed below. In addition, the pulse-like nature of longer-period components of the Love wave or  $G$  wave is brought out by low-pass filtering.

High-pass filtering is also useful in certain applications. L. Sykes (personal communication) used the equipment described here to successfully isolate, by high-pass filtering, the higher-

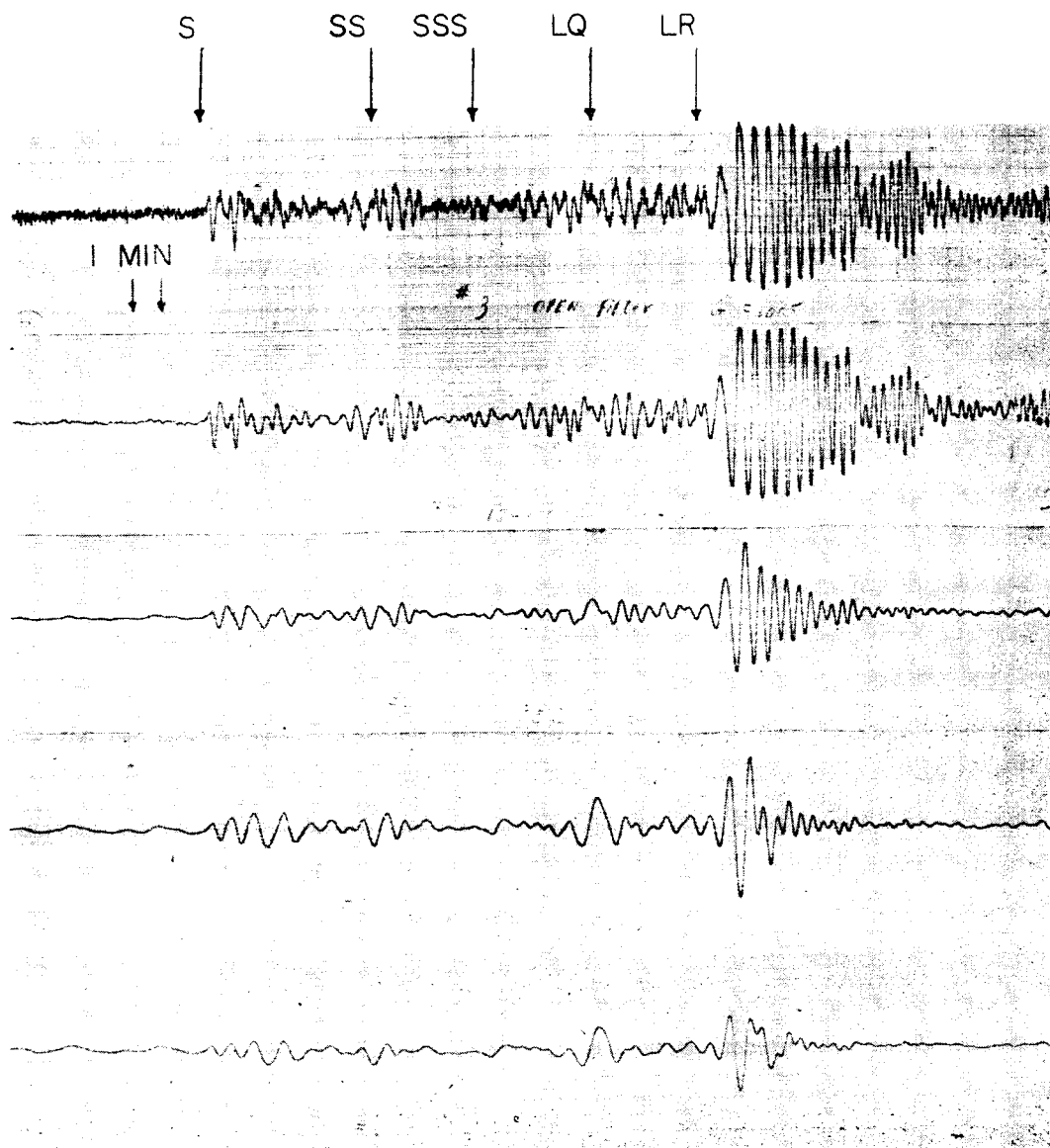


Fig. 4. N-S seismograms of South Pacific earthquake. Low-pass filter corners, open, 15, 32, 48 and 60 seconds, from top to bottom.

mode surface waves from the fundamental-mode surface waves for use in a study of oceanic surface wave dispersion. Sykes used magnetic tape seismograms produced from original photographic records with the converter discussed earlier. Band-pass and band-rejection filtering, although not illustrated here, are being used to emphasize or reject specific portions of the frequency spectrum.

The records shown in Figure 5 illustrate a method of eliminating filter phase shift. In all the previous figures showing filtered seismograms, the reproduced magnetic tape seismogram was passed through a filter and recorded directly on a visible recorder. Both the amplitude and phase response of the filter are introduced into these records. For some purposes this

is desirable, since the arrival time and the direction of the 'first break' of a transient signal are preserved. In other cases, particularly when phase velocity studies are contemplated, the strong phase shifts normally associated with sharp filters are undesirable. Sharp filtering without any associated phase shift can be obtained by reproducing the signal from the original magnetic tape, passing this signal through a given filter, and re-recording the output from the filter on another magnetic tape. The re-recorded tape is then inverted on the tape transport in order to produce a seismic signal in negative time, i.e., from end to beginning. This signal is then passed through the same filter and played out on a visible recorder. In this way, the amplitude response of the filter is squared and the phase

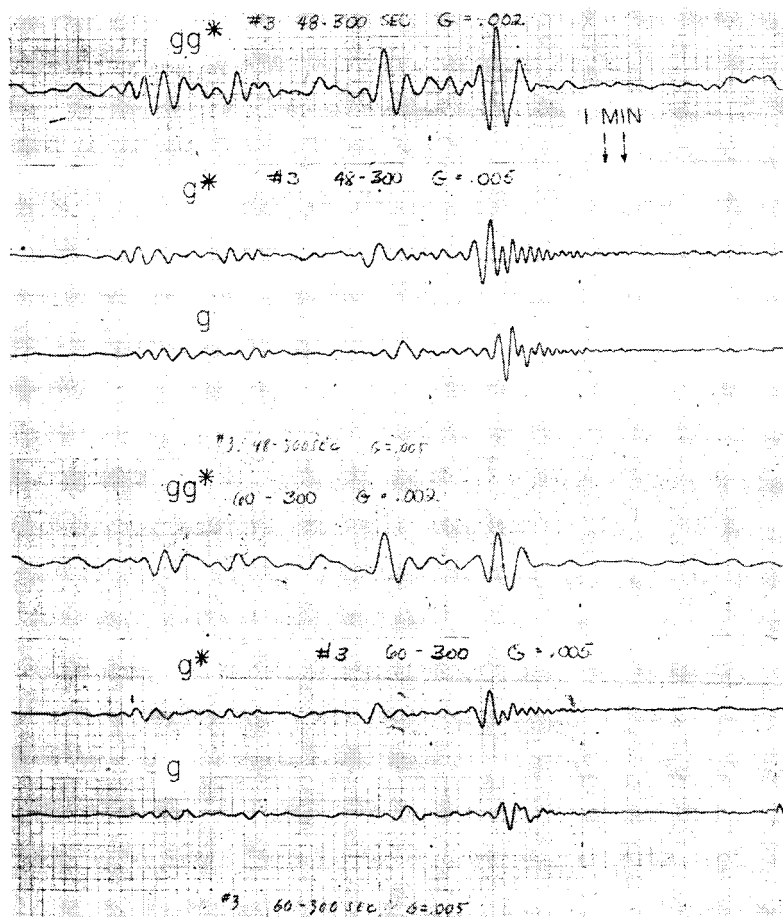


Fig. 5. N-S seismograms of South Pacific earthquake illustrating removal of filter phase shift. Low-pass filter corners, 48 seconds on the three upper traces, 60 seconds on the three lower traces;  $g$ , normal filter phase shift,  $g^*$ , negative phase shift,  $gg^*$ , no phase shift.

shift is completely canceled (see appendix 1). In Figure 5 the bottom trace of each set of three records represents the filter output from the original magnetic tape seismogram. The frequency components of the signal are multiplied by the filter transfer function,  $g(\omega)$ .

The middle traces were obtained by reproducing the original seismogram through the filter in negative record time. In this case, the frequency components are multiplied by  $g^*(\omega)$  and the filter phase shift is reversed. Filtered signals with no phase shift, multiplied by  $gg^*$ , are shown in the upper traces. These records are aligned in time so that an examination of the records quickly reveals the effects of the filter. In positive time, the filter introduces a delay in the response; in negative time, it can be seen that the filter produces a time advance. In the record free from filter phase shift, it may be seen that the apparent inverse dispersion mentioned earlier is not noticeable in the  $S$  wave but can still be observed in the Rayleigh wave train.

An important conclusion to be drawn from this last figure is that the double filtering method or some substitute should be used for precise measurements of group and phase arrival times for frequencies near filter corners to ensure that observed phenomena are not the result of the phase response of the filter network used. The effect of seismograph response on recorded transient signals has been examined by *Landisman et al.* [1959].

*Inverse filtering.* Before using the selective filtering described above or other analyses, it is frequently desirable to eliminate the response of the recording instrument from the seismogram or to preshape the signal to some desired characteristic. Either operation is possible by passing the signal through the desired inverse filter, built from analog computer components. In practice, this can be accomplished by selecting the desired response, determining the characteristics of the required inverse filter, determining the transfer function of this filter, programming the function on the analog computer, and using the computer as the filter. System noise obviously places practical limitations on this procedure. Examples of the effect of inverse filtering are presented in Figures 6 and 13. In both cases, the original seismogram was recorded directly from a critically damped seismometer with a natural period of 15 seconds. The magnification of the system

decreases at 6 db/octave, with increasing period, out to 15 seconds and beyond this at 18 db/octave. The response desired for these cases is constant sensitivity to particle velocity, equivalent to a decrease in magnification of 6 db/octave with increasing period. This is obtained out to a period of 200 seconds, beyond which the magnification returns to the original 18-db/octave slope. The inverse filter used for this purpose is flat with increasing period to 15 seconds; it increases at 12 db/octave to 200 seconds and is flat at longer periods.

The transfer function of this inverse filter, in transform notation, is

$$g(s) = (s + \omega_0)^2 / (s + \omega_f)^2$$

where  $\omega_0$  is the natural angular frequency of the pendulum and  $\omega_f$  is the angular frequency equivalent to a corner period of 200 seconds.

This equation can be programmed using seven operational amplifiers, four of which are used with integration networks. In Figure 6,<sup>3</sup> the trace labeled 'particle velocity' clearly shows the increase in long-period response produced by the inverse filter. This increase is also evident in the trace labeled 'V' in Figure 13. The resultant signals are used for the energy studies outlined below. This procedure is not limited to producing velocity traces but may be used to provide any reasonable amplitude and phase response.

Given a record in the frequency domain  $R(\omega) = S(\omega)f(\omega)$ , where  $f(\omega)$  represents the earth motion and  $S(\omega)$  represents the seismograph response characteristic, a new record  $R'(\omega)$  with an equivalent filtering  $g(\omega)$  can be obtained by putting the record through a filter whose transfer function is  $g(\omega)/S(\omega)$ ; that is,

$$R'(\omega) = (g(\omega)/S(\omega))R(\omega) = g(\omega)f(\omega)$$

[*Bogert*, 1961a].

*Spectral analysis.* With the original seismogram recorded on magnetic tape, there are several ways to perform spectral analyses. Figure 7 is a block diagram showing two alternative ways of obtaining frequency spectrums. Along the upper path, the seismogram is passed through a band-pass filter with variable center frequency,

<sup>3</sup> The time base of this and succeeding seismograms, except those in Figure 13, is compressed by a factor of 64.

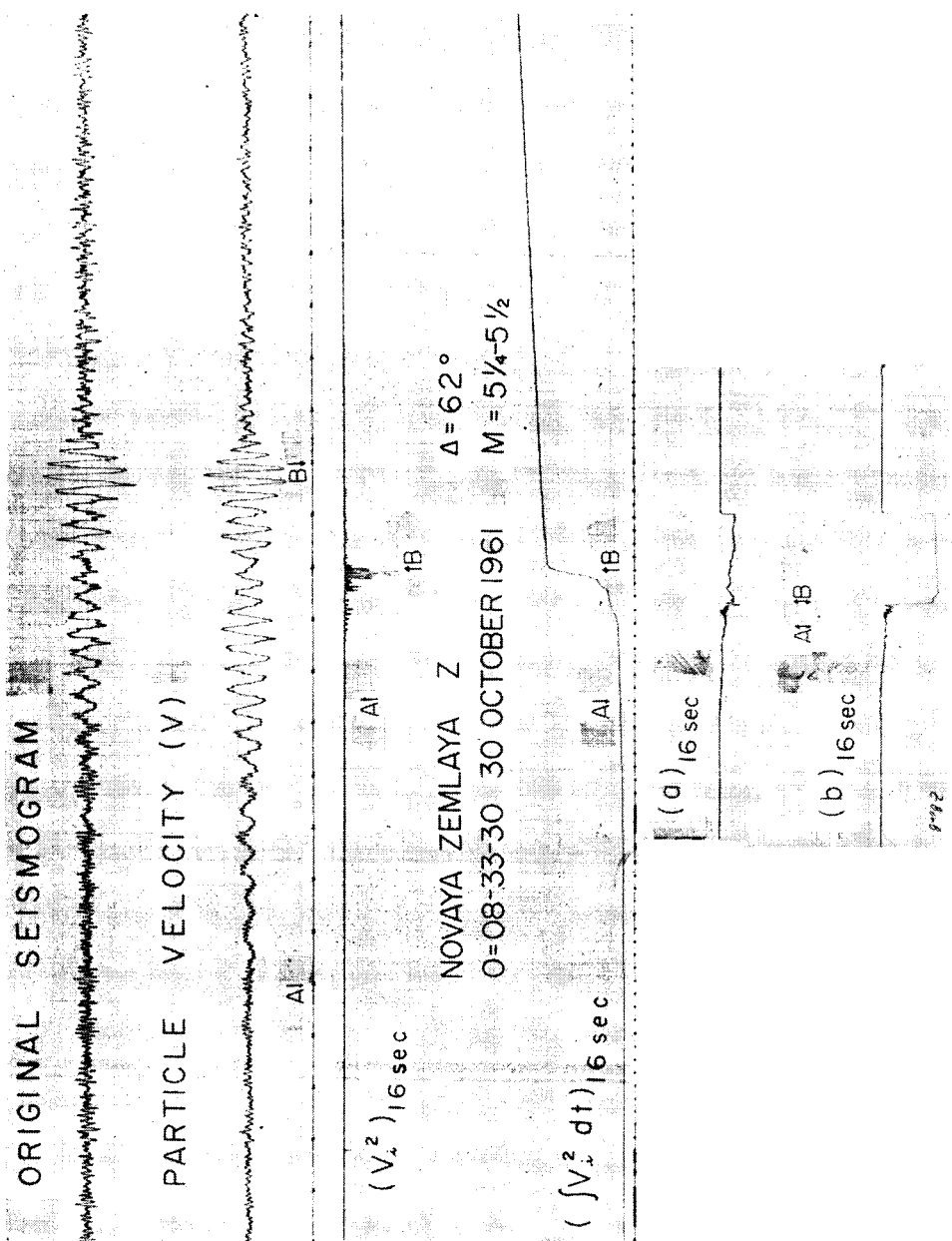


Fig. 6. Vertical records of Novaya Zemlya explosion illustrating inverse filtering and two methods of spectral analysis. Points A and B on the three pairs of records are at same times; time marks, 1 second apart in analysis time, are 64 seconds apart in original record time.

## CUMULATIVE ENERGY AND FOURIER COEFFICIENTS

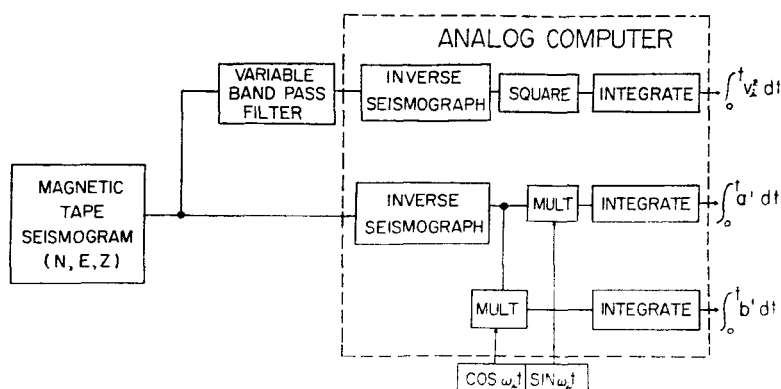


Fig. 7. Block diagram of alternative methods for analog spectral analysis.

$\omega_i$ , into an analog computer. In the analog computer, the first operation is to provide a response which is flat to particle velocity. The output of the inverse seismograph,  $v_i$ , is then squared and integrated. This integral provides a measure of the energy in a given frequency band as a function of time. An energy spectrum (per unit bandwidth) is obtained by measuring the total value of the integral for a given transient signal for several frequency bands and plotting these values as a function of frequency. Cumulative energy as a function of time will be discussed below. The resolution of this method of determining spectrums depends on the bandwidth of the filter used.

In the frequency domain the output of the band-pass filter,  $h(\omega)$ , is given by

$$h(\omega) = g(\omega)f(\omega)$$

where  $f(\omega)$  is the transform of the input signal and  $g(\omega)$  is the filter transfer function. Since  $g$  approaches zero outside the filter passband,  $h$  will also approach zero outside the same passband, provided that  $f$  is well behaved. From Parseval's theorem

$$\int_{-\infty}^{\infty} F^2(\tau) d\tau = \int_{-\infty}^{\infty} G^2(\omega) d(\omega)$$

where  $G(\omega)$  is the Fourier transform of  $F(\tau)$ . When the output of the inverse seismograph,  $v_i$ , is zero for times less than zero and greater than  $t$ , we get

$$\int_{-\infty}^{\infty} v_i^2 d\tau = \int_0^t v_i^2 d\tau = \int_{-\infty}^{\infty} h^2 d\omega$$

and, assuming  $g = 1$  and  $f = f_a$  within the filter passband,

$$\begin{aligned} \int_{-\infty}^{\infty} h^2 d\omega &\simeq \int_{\omega_1}^{\omega_2} f_a^2 d\omega \\ &\simeq f_a^2(\omega_i)[\omega_2 - \omega_1] = f_a^2(\omega_i)\Delta\omega \end{aligned}$$

where  $\omega_1$  and  $\omega_2$  are the filter corner frequencies and  $\omega_i$  is the center frequency. Therefore, the Fourier amplitude  $f(\omega_i)$  is approximated by

$$f_a(\omega_i) = \left[ \int_0^t v_i^2 d\tau \right]^{1/2} / (\Delta\omega)^{1/2}$$

Since the filters generally used have a constant  $Q$ , i.e.,  $\Delta\omega = \omega_i/Q$ , we get finally,

$$f_a(\omega_i) = \left[ \int_0^t v_i^2 d\tau \right]^{1/2} Q^{1/2} / \omega_i^{1/2}$$

Thus, to obtain Fourier amplitudes by this method, it is necessary either to divide the integral by the square root of the filter bandwidth or to multiply by  $Q^{1/2}/\omega_i^{1/2}$ .

The  $f_a(\omega_i)$  obtained in this manner are approximately the root mean square of the Fourier amplitudes of the input signal over the filter passband, and they approach the exact value,  $f(\omega_i)$ , as the filter bandwidth approaches zero.

This type of analysis was performed on the seismogram (vertical-component instrument) of the large Soviet nuclear explosion of October 30, 1961, as pictured in Figure 6. The result of the squaring operation is shown as  $(v_i^2)_{16 \dots}$  where the subscript, 16 sec, indicates a 1-octave filter passband centered at 16 seconds. The integrator output for 16 seconds is also shown in this figure.

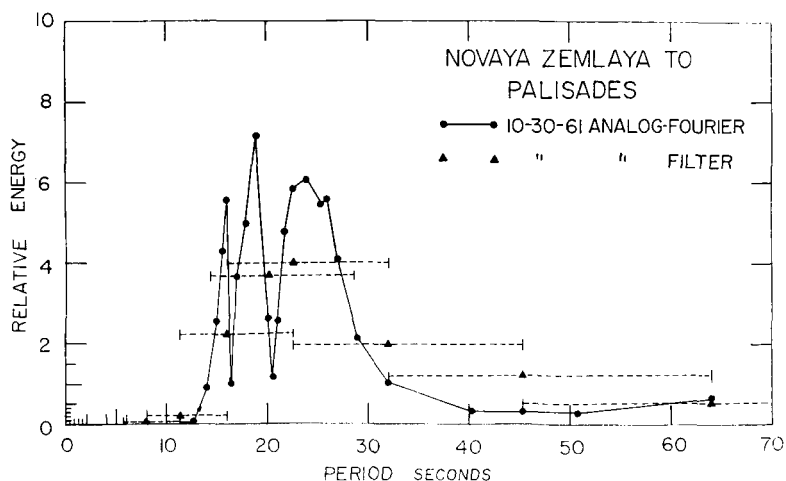


Fig. 8. Energy spectrum of Palisades seismogram of Novaya Zemlya explosion obtained by band-pass filter and Fourier methods. Dashed lines represent filter passband.

In Figure 8, the results of this analysis  $[f_s(\omega_i)]^2$  are compared with the square of the Fourier amplitude spectrum. The horizontal dashed lines represent the filter bandwidth used. As can be seen in Figure 8, the bandwidth of the filter is relatively broad, and only general features of the spectrum are resolved. Also, it is obvious that in this case the amplitudes are not constant within all the filter bands used.

To obtain a more detailed spectrum, the magnetic tape seismogram is reproduced directly into the analog computer following the lower path in Figure 7. The output of the inverse seismograph is multiplied separately by  $\sin \omega_i t$  and  $\cos \omega_i t$ , and the resultant products are integrated. (A simple three-amplifier circuit can be used to generate  $\sin \omega_i t$  and  $\cos \omega_i t$  within the analog computer.)

The integrals thus obtained,

$$\int_0^t \begin{Bmatrix} a' \\ b' \end{Bmatrix} d\tau = \int_0^t f(\tau) \begin{Bmatrix} \cos \omega_i \tau \\ \sin \omega_i \tau \end{Bmatrix} d\tau$$

are equal to the Fourier coefficients of  $f(t)$

$$\begin{Bmatrix} a(\omega_i) \\ b(\omega_i) \end{Bmatrix} = \int_{-\infty}^{\infty} f(\tau) \begin{Bmatrix} \cos \omega_i \tau \\ \sin \omega_i \tau \end{Bmatrix} d\tau$$

when

$$f(t) = \begin{cases} 0 & \tau < 0 \\ f(\tau) & 0 < \tau < t \\ 0 & \tau > t \end{cases}$$

That is, the integrals give exactly the Fourier coefficients of a seismic signal commencing at or after  $\tau = 0$  and set equal to zero at  $\tau = t$ . Similarly, the Fourier coefficients for a portion of the signal between times  $t_1$  and  $t_2$  (the signal is assumed to be zero outside this interval) are given by the difference between the values of the integral at  $t_2$  and at  $t_1$ . Provided that the background microseisms are coherent and have a constant power spectrum, the values of  $a$  and  $b$  for the signal can be obtained exactly by measuring  $a$  and  $b$  from the sloping base line produced by the background energy.

The Fourier amplitude  $f(\omega_i)$ , obtained approximately in the previous method, is given by  $f = (a^2 + b^2)^{1/2}$ . Of course,  $f$  and the spectral energy,  $f^2$ , can be obtained at the output of the computer if desired (provided that enough computer elements are available). However, all phase information and the ability to eliminate coherent background completely are lost unless  $a$  and  $b$  are observed separately.

The integrals for  $a$  and  $b$ , evaluated at a period of 16 seconds, for the Soviet nuclear explosion are shown at the bottom of Figure 6. The values of the square of the Fourier amplitudes are plotted in Figure 8 for comparison with the points obtained by the approximate method.

A simple analog method for obtaining the Fourier coefficients without the use of multipliers and oscillators is described by Cooper and Broom [1961]. This method was also used to obtain Fourier coefficients for the nuclear explosion of October 30, 1961, and the results, al-

though not presented in this paper, are in agreement with the results obtained by the method outlined above.

In Figure 9, the Fourier amplitudes obtained by the analog method described above are compared with two spectrums from the large Soviet nuclear explosions of 1958, as calculated on a digital computer by *Pomeroy* [1963]. Within the accuracy to which the epicenters are known, the propagation paths for all three events are identical. The most remarkable feature of this comparison is the similarity of the three spectrums. The agreement of details among the three explosions is excellent. The sharp minimums in all of the spectrums around 16.5 and 20.6 seconds are probably due to interference resulting from multipath propagation. The only definite difference between the spectrums is that the 1961 Soviet explosion, which apparently was the largest to date, is richer in the long-period components. The difference in response between the recording instruments used does not affect this conclusion. The over-all level of the spectrum of the 1961 event was higher, but it has been normalized approximately to the maximum level of the smaller 1958 events.

Rough power spectrums may be obtained with simple components in the following manner. A certain length of the incoming recorded signal is passed through a narrow-band filter and recorded on a visible recorder; the average amplitude recorded on the visible recorder for the

time and frequency interval selected is then squared. This value is a measure of the power in the band passed by the filter. The resolution of this method depends on the bandwidth of the filter used. This simple technique is useful in the study of microseisms and other background noise.

A hurricane, named Donna by the U. S. Weather Bureau, struck the east coast of the United States early on September 11, 1960. Figure 10 shows the position of the storm center every 12 hours starting at 0600 UT, September 11, 1960. The numbers on the map associated with storm positions, e.g., the 10 at 0600 of September 12, 1960, refer to the wind velocity at Palisades in knots. Using the simple method for obtaining power spectrums outlined above, we obtained the power spectrums of microseisms that were recorded when the storm was at positions 1, 2, 3, and 4 (numbers in the squares of Figure 10). These spectrums are plotted in Figure 11. Since the filter used has a 1-octave pass-band, the spectral densities shown are in power per octave. A time interval of approximately 1 hour at each position was used, and the average amplitude, excluding anomalously high amplitudes, was obtained.

The over-all level of the microseismic noise in the period range of 3 to 7 seconds increased by approximately a factor of 5 between positions 1 and 2. For periods between 10 and 20 seconds, the level of the background increased by a factor

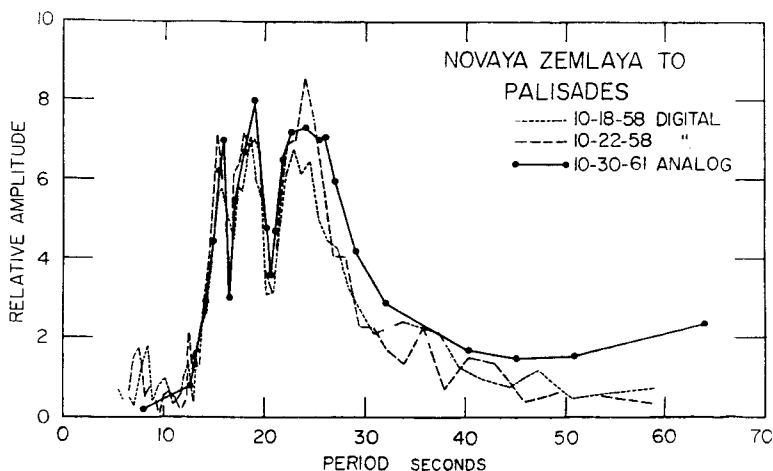


Fig. 9. Amplitude spectrums of three Novaya Zemlya explosions. Solid line is from magnetic-tape seismogram of October 1961 event; dashed lines are from digital analysis of photographic records of two October 1958 events.



These curves are related to cumulative energy through relationships which depend upon wave type, angle of incidence, and group velocity. They are rather complex, but they contain a considerable amount of useful information.

In Figure 6, we see that energy in the band around 16 seconds continues to arrive at a slowly decreasing rate for at least 20 minutes after the arrival of the slowest Rayleigh wave. In Figure 12 differences in rate and total accumulation as a function of time between different components for an octave band around 16 seconds are illustrated. In Figure 13 it is shown that most of the energy in a given frequency band arrives at discrete times, but the wide-band signal arrives at a rather uniform rate. Most of the energy is concentrated near 8 seconds period.

Although most of these characteristics are already well known, this form of presentation makes it easy to compare the effects of magnitude, focal depth, epicentral distance, and seismic path on seismic signals. Group velocities of various modes of propagation as a function of period can be obtained from this type of display. The arrival times for the particular period are represented by the maximums of slope. The group arrival times obtained from  $\int v_g dt$  are somewhat delayed by filter phase shift, but, as we have already explained, the delay can be eliminated.

*Rotation of axes and phase identification.* A method of separating earthquake phases by particle motion is shown in Figure 14. The output of the magnetic tape seismogram is played into potentiometers in the analog computer whose values are set to the sine and cosine of the azimuth angle,  $\theta$ , from the station to the event under study. Pure longitudinal and transverse traces are produced from the N-S and E-W records by the transformation

$$T = N \sin \theta - E \cos \theta$$

( $T$  positive to right of path from epicenter)

$$L = N \cos \theta + E \sin \theta$$

( $L$  positive toward epicenter)

where  $T$  is the transverse record and  $L$  is the longitudinal record. If the longitudinal and vertical traces are multiplied, the product,  $LZ$ , defining 'away' and 'up' motions as positive, is positive for compressional-type particle motion and

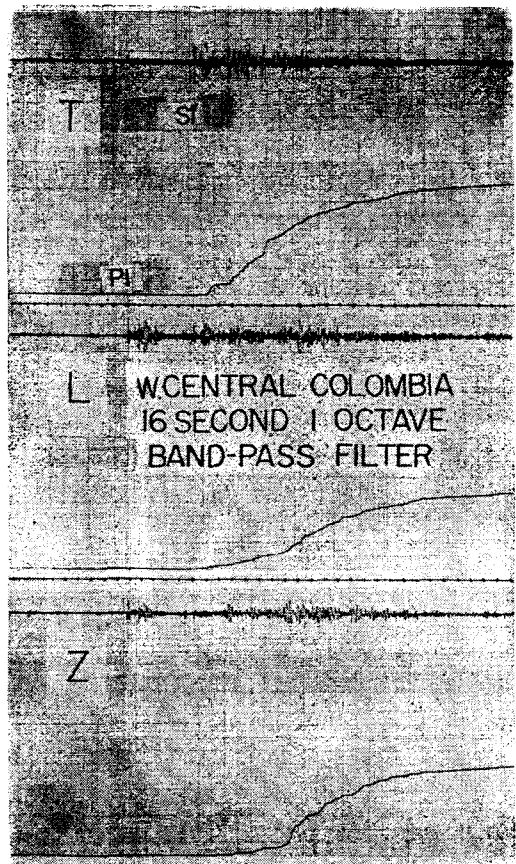


Fig. 12. Transverse horizontal,  $T$ , longitudinal horizontal,  $L$ , and vertical,  $Z$ , seismograms (unfiltered) from west-central Colombia earthquake compared with integral of the square of the same component of the particle velocity in a 1-octave band centered at 16 seconds; 64 seconds record time per time mark.

negative for  $SV$ -type particle motion. Pure Rayleigh wave motion goes positive and negative at twice the original frequency. At some incidence angles, incident  $SV$  produces Rayleigh-type surface particle motion. This simple procedure separates transverse horizontal ( $T$ ), longitudinal horizontal ( $L$ ), compressional, vertically polarized transverse, and longitudinal elliptical (Rayleigh-type) surface particle motions. It is possible with this method to obtain any set of axes desired, including off-vertical axes, if required. The product  $LZ$  may be integrated to improve the signal-to-noise ratio for the body waves, since any 'pure surface wave' microseisms which may be present will integrate to zero. A brief discus-

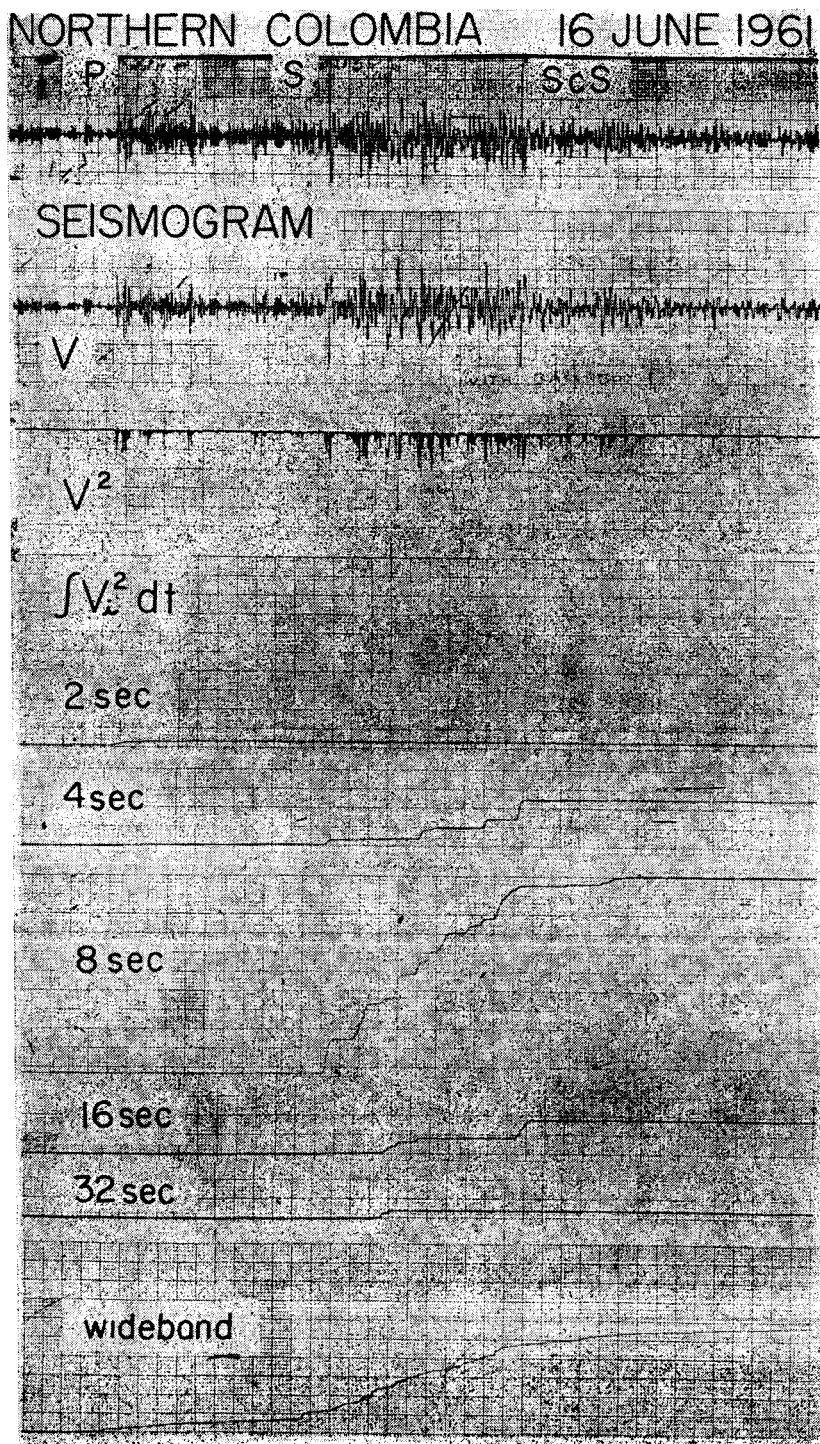


Fig. 13. Cumulative signal on E-W component at various periods (1-octave band) as a function of time from northern Colombia earthquake; effects of inverse filtering can be seen by comparison of upper two traces; 32 seconds record time per large division.

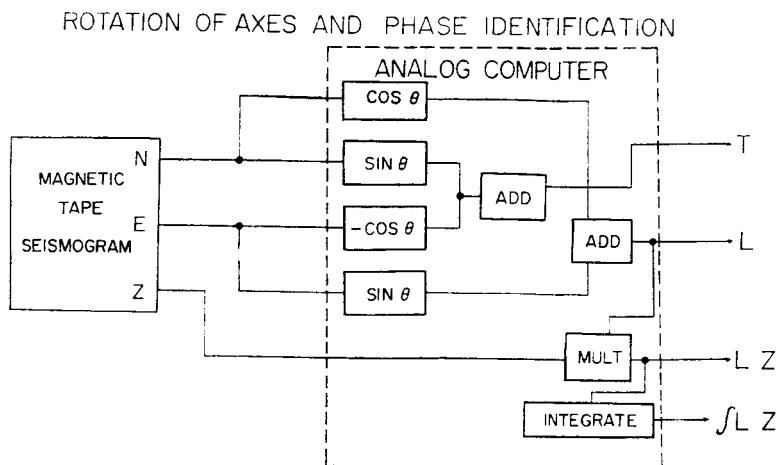


Fig. 14. Block diagram of circuitry used to obtain longitudinal and transverse components of horizontal motion and to further separate earthquake phases by particle motion.

sion of the effects of differences in instrumental amplitude and phase response on this procedure is given in appendix 2.

In Figure 15 the Rat Islands earthquake of December 30, 1961, provides an example of the use of this procedure. The azimuth at Palisades is  $321.2^\circ$ . Playbacks of the original N-S and E-W seismograms are shown in the two top traces. The next two traces show the transverse and longitudinal horizontal motion. The *P* waves are essentially removed from the transverse component, as we would expect. The *SH* waves appear to arrive about 10 seconds later than the *SV* waves. Most of the later surface waves are overloaded, but these are not essential in this study. On the bottom trace, *LZ*, the *P* wave arrival is sharply defined and most of the particle motion preceding *S* is of the compressional type; i.e., most of the trace is displaced upward. Some *SV*-type motion, indicated by downward trace displacement, is observed 21 seconds after the initial *P* motion. This might be an *SV* wave, derived from incident *P* at the surface, reflected to the *M* discontinuity and back [Sharpe, 1935]. The first *S* arrival is clearer on the *LZ* than on any of the individual traces. Several phases with compressional-type particle motion are observed following *S*, and some of these may be surface-reflected phases arriving as *P*. The arrival at about the predicted arrival time for *PKKP* agrees with *P*-type motion arriving from the direction away from the epicenter, as it should for *PKKP*.

In Figure 16 another example of axis rotation and phase identification is presented. This earthquake occurred in west-central Colombia on December 20, 1961, at an azimuth of  $182.9^\circ$ , i.e., almost due south. Although the axis-rotation technique was used, the original azimuth is such that the recording axes were essentially longitudinal and transverse, and no further separation was apparent. In the *LZ* product trace, the particle motion can be seen to be very 'pure'; i.e., little multiply reflected *SV* or surface wave energy is generated in the vicinity of the station. The initial *P* wave is quite distinct in the original records and on the product trace. It does not appear that integration of the product trace would increase the signal-to-noise ratio at the initial *P* time in this case. The initial *S* arrival is also quite clear.

Playbacks of the magnetic tape seismograms from an earthquake which occurred on the west coast of Chile on February 14, 1962, are shown in Figure 17. On this record the earlier arrivals are clearly *P* waves; the *S* wave arrival is quite sharp, and several phases following *S* are clearly defined. There are several arrivals immediately following *S*, some of which may correspond to multiple surface reflections terminating as compressional waves. Of particular interest are the two sharp phases arriving at about the predicted arrival times for *PKPPKP* and *PKSPKP*. These phases show particle motion opposite in sense to the initial *P*, as is required for such phases, since these waves approach the recording station from

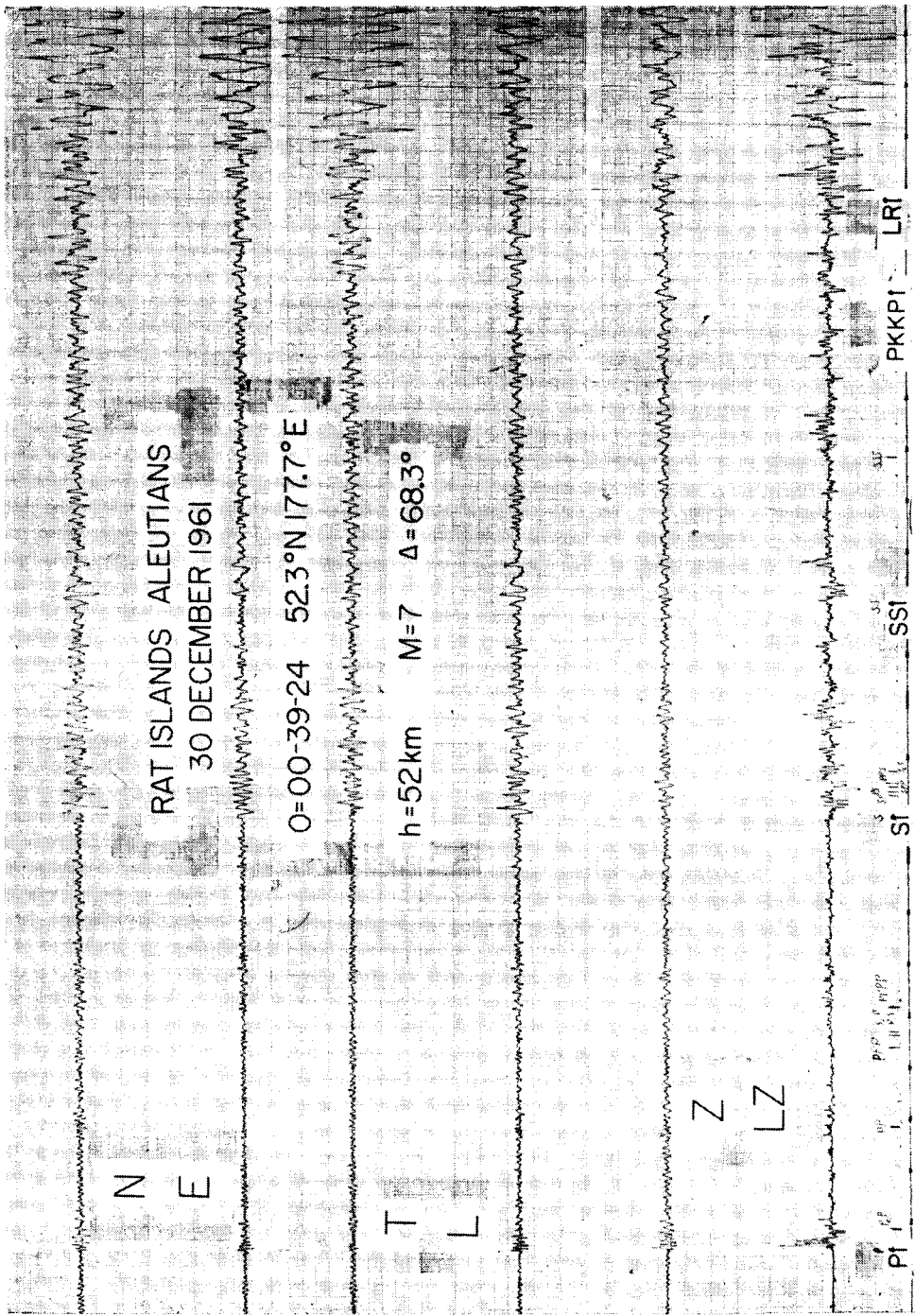


Fig. 15. Seismograms of Rat Islands earthquake illustrating separation of longitudinal and transverse horizontal motion and *P* and *SV* types of particle motion. The time scale on this and all succeeding figures is 64 seconds per time mark.

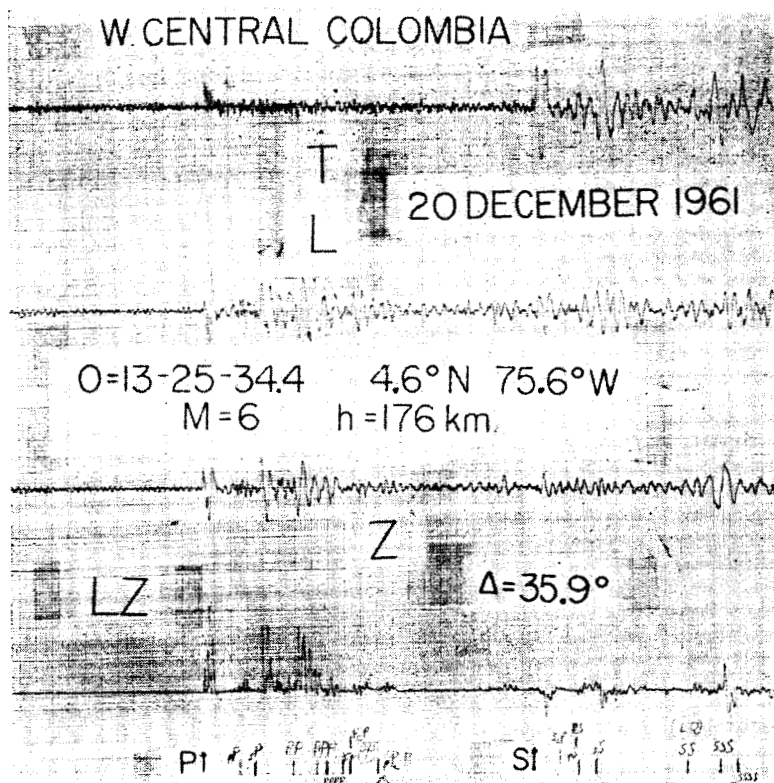


Fig. 16. Seismograms of west-central Colombia earthquake.

the opposite direction. These phases appear to be more distinct on the product trace than on the original records. Also, the doubling of the frequency produced by the multiplication tends to sharpen the arrivals and to increase the precision with which arrival times can be determined.

Figures 18 and 19 show phase separation achieved for Palisades seismograms of the Iranian shock of September 1, 1962. The azimuth at Palisades is  $42.6^\circ$ . There are no sharp phases on the transverse component before the arrival time of S; however, starting about 3 seconds after P, there is a considerable amount of short-period

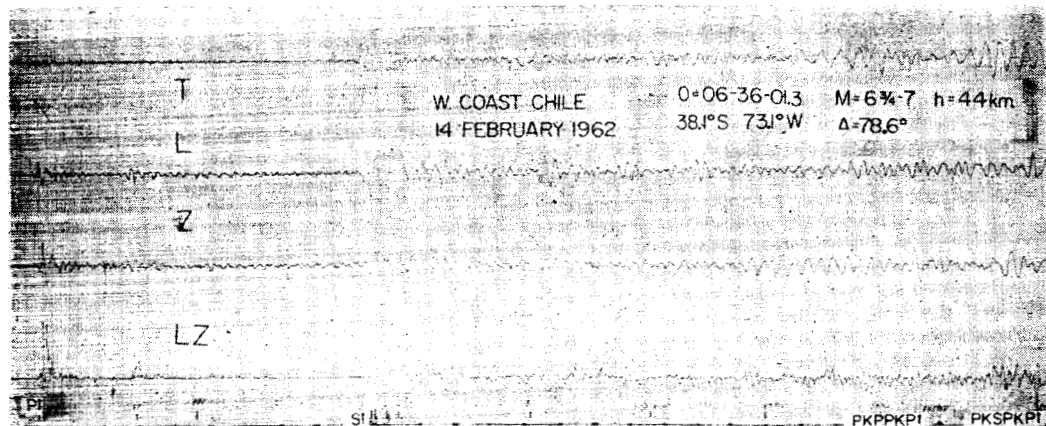


Fig. 17. Seismograms of west-coast Chile earthquake.

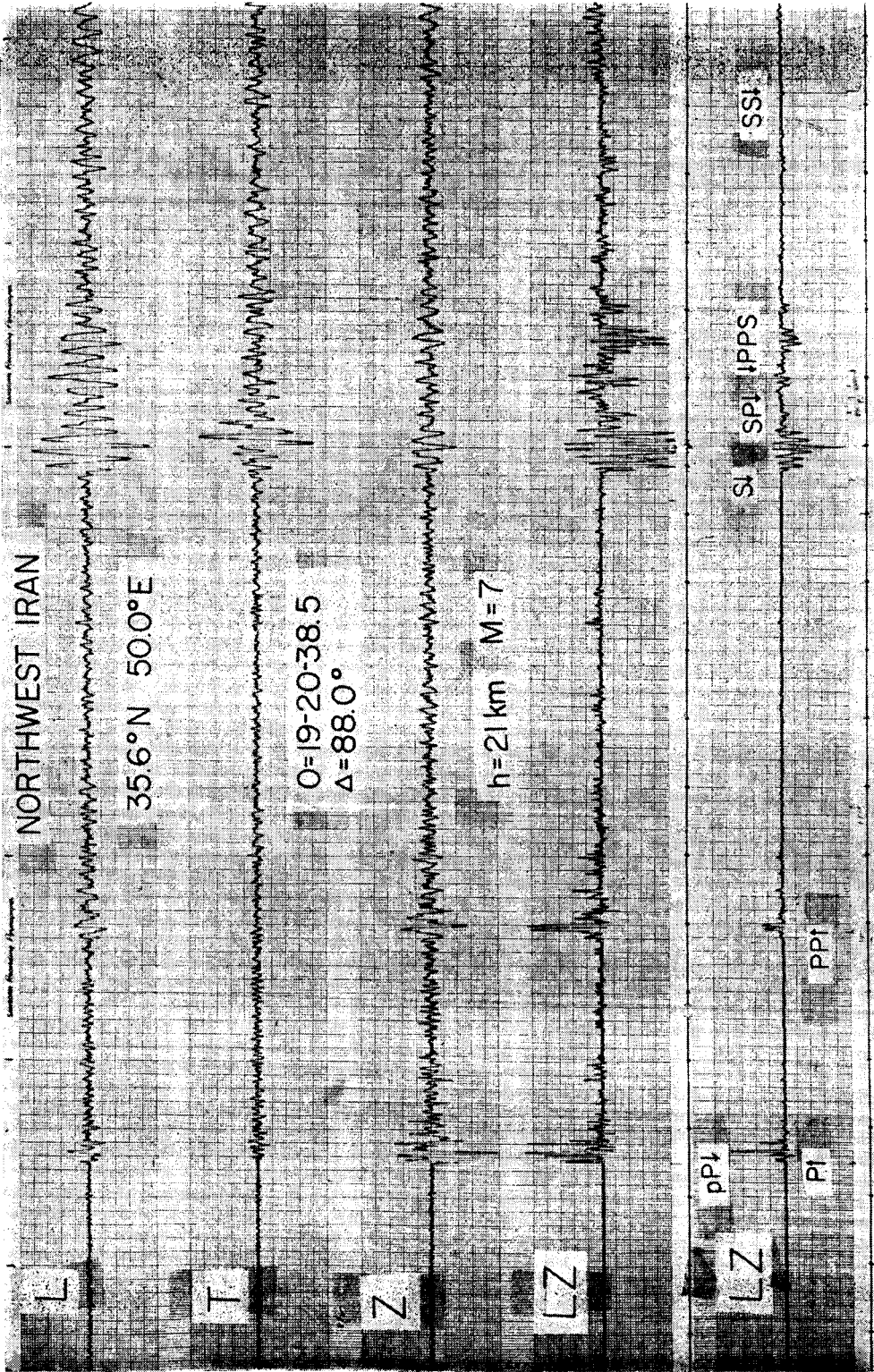


Fig. 18. Seismograms of northwest Iran earthquake showing body phases with two gain levels for LZ product.

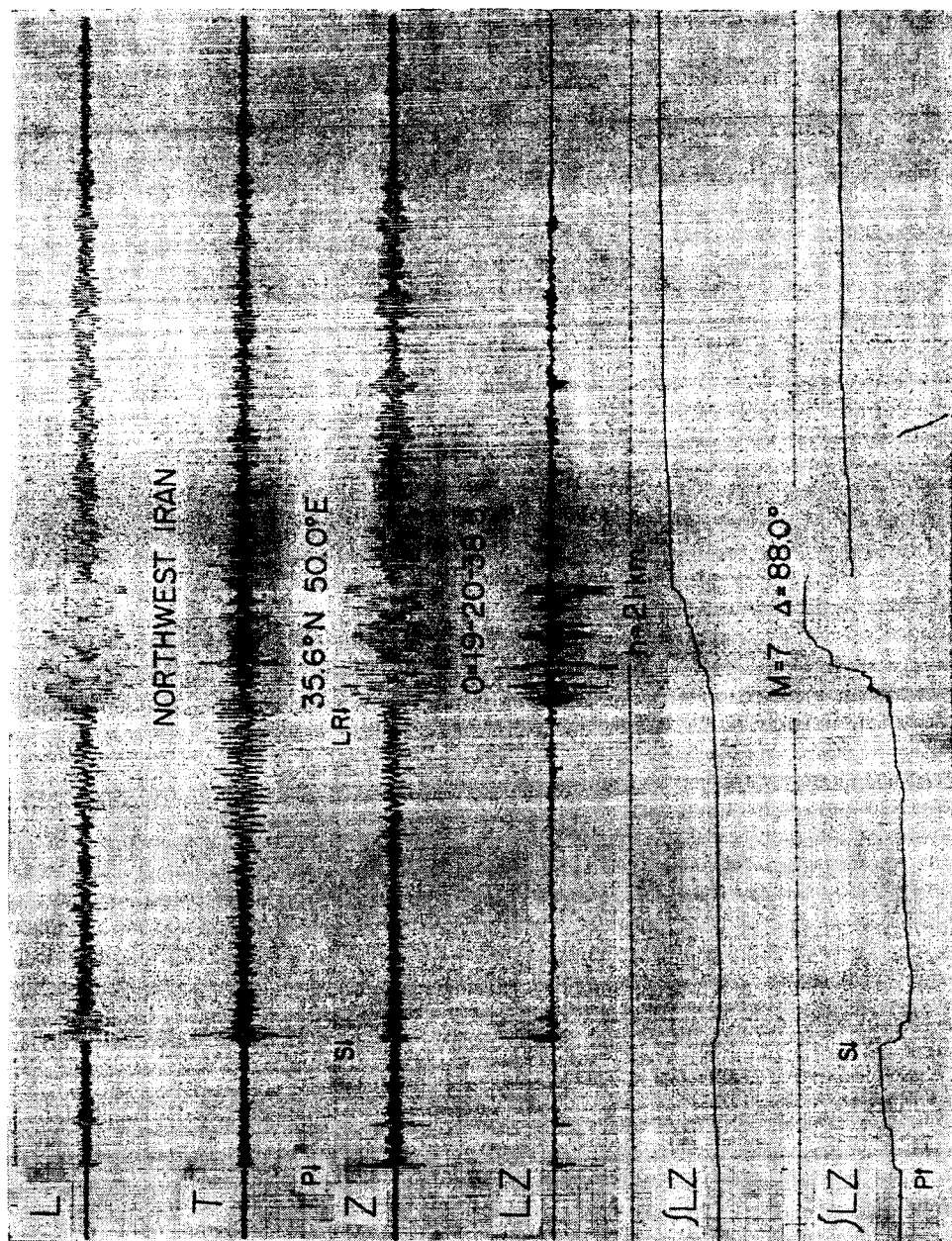


Fig. 19. Seismograms of northwest Iran earthquake showing both body and surface waves; the two lower traces are two levels of time integral of LZ product. Note that the LZ trace is of opposite sign to those presented previously.

energy on the transverse component. No significant improvement could be obtained by modifying the apparent azimuth of arrival and the relative amplitudes of the two horizontal components. A product of the vertical and transverse components, not shown here, indicates little coherence. Figure 18 shows the body waves on an expanded scale with two gain levels for the *LZ* product trace.

The entire seismogram is shown in Figure 19. Here the time scale is 1/5 that in the preceding figure. The Rayleigh waves in the *LZ* product trace are approximately symmetrical about the time axis at twice the signal frequency, as expected. The asymmetry shown represents a phase shift from the theoretically expected value for traveling waves. In the last large burst in the Rayleigh wave train, the asymmetry is equivalent to a phase shift of about 20°. This value is four times greater than the known instrumental phase error.

The two lower traces are two gain levels of the time integral of *LZ*. Under certain conditions this type of display can sharpen the body wave arrivals and improve the signal strength relative to the background microseisms.

**Vibration analysis.** Effective use of vibration and sonic analyzers in the audio-frequency range can be made when analog seismic signals are recorded on magnetic tape. Such analyzers as the Kay Electric Company's Missilyzer produce a plot of frequency versus time, i.e., group arrival time, if a signal in the suitable frequency range is provided. Since this type of analyzer works in the audio-frequency range, it is generally necessary to compress the time scale to bring all the long-period signals of interest into a useful frequency band. Vibration analyses of earthquake and explosion signals have been made by *Ewing et al.* [1959, 1961a, b]. A study of microseisms using this instrument with the output from magnetic tape seismograms has been reported by *Page and Oliver* [1963].

#### CONCLUSIONS

The examples of analog reduction and analysis of magnetic tape seismograms presented in this paper illustrate some of the advantages of this kind of recording. Relatively simple and rapid analog procedures are available which can often produce the desired information from the raw data in a form most useful to the observer.

Among such procedures, not discussed in this paper, are determinations of azimuth and angle of incidence as functions of time, total particle amplitude versus time, and various types of running spectrums.

Detailed studies of particle motion and spectrums of body waves may permit us to separate near-station effects from those of the source and propagation path. *Haskell* [1962] presented theoretical values of surface motion from emergent *P* and *SV* waves. Comparison of these with observed motions will be of considerable interest [*Cook et al.*, 1962].

The *P* waves, including the later arrivals, from the distant shocks presented in this paper exhibit rather pure *P*-type particle motion. A small amount of apparently scattered transverse horizontal motion does not appreciably affect the coherence of the longitudinal horizontal and vertical motions. The beginnings of the *S* waves are equally easy to identify by particle motion. For these reasons, the accuracy and reliability of *P* and *S* wave identification and arrival-time measurements can be improved by using a record of the product of the longitudinal horizontal and vertical motions in conjunction with a record of transverse motion. The recognition of *P* wave motion in the presence of surface wave background noise can be facilitated by examining the integral  $\int LZ dt$  as a function of time.

The dynamic range, stability, and reliability of magnetic tape systems are continually improving, as are analog computing elements. Also, the dynamic range required of a system can be reduced by a judicious preshaping of the transducer output. The relatively small amount of information on which digital processing might be desired can be digitized quite easily from analog magnetic tape records at a sampling interval selected for the problem at hand.

#### APPENDIX 1

The following equations in the frequency domain outline the procedure for eliminating phase shifts.

The input signal may be expressed as

$$f(\omega) = re^{i\theta}$$

and the filter transfer function is given by

$$g(\omega) = ae^{i\phi}$$

In general  $r$ ,  $\theta$ ,  $a$ , and  $b$  are functions of  $\omega$ . The filter output, then, is

$$h(\omega) = f(\omega)g(\omega) = are^{i(\theta+b)}$$

Inverting the filtered signal in the time domain is equivalent to changing the sign of the phase angle. The filtered seismic signal in negative time is given by

$$f'(\omega) = h^*(\omega) = are^{-i(\theta+b)}$$

Refiltering this signal we obtain, at the output,

$$h'(\omega) = f'(\omega)g(\omega) = a^2re^{-i\theta} = f^*gg^*$$

Thus, the signal has been multiplied by the square of the filter amplitude characteristic, and the original signal phase is preserved. The negative phase angle merely indicates that the record is obtained end first.

#### APPENDIX 2

Differences in instrumental phase and amplitude response obviously can produce errors in the results of analyses in which various combinations of the originally recorded components of a signal are used. Theoretically, accurate calibration and subsequent correction for differences in response can eliminate these errors. In practice, however, fairly carefully matched instruments can and should be obtained.

Original recording of two orthogonal horizontal components and a vertical component is desirable, since this automatically separates certain types of waves without further transformation. Differences in electromechanical details of the transducers are unimportant as long as the over-all amplitude and phase responses of the recordings are matched [Espinosa *et al.*, 1962].

To determine the effects of phase and amplitude differences between components, we shall first assume that the longitudinal and the tangential horizontal motions have been separated, and we shall examine the response of the  $LZ$  product to  $P$ ,  $SV$ , and Rayleigh waves.

*P waves.* A frequency component of the earth motion may be given by

$$L = L_0 \cos \omega t \quad Z = Z_0 \cos \omega t$$

where  $L$  and  $Z$  are defined as positive away from the epicenter and up.

The instrument outputs are given by

$$L' = GL_0 \cos(\omega t - \phi)$$

$$Z' = \beta GZ_0 \cos(\omega t - \phi - \epsilon)$$

where  $G$  and  $\phi$  are the amplitude and phase response of the longitudinal component and  $\beta$  and  $\epsilon$  are the fractional gain and phase lag between the vertical and longitudinal components. The product is

$$L'Z' = \beta G^2 L_0 Z_0 \cos(\omega t - \phi) \cos(\omega t - \phi - \epsilon)$$

or

$$L'Z' = \frac{\beta G^2 L_0 Z_0}{2} [\cos \epsilon + \cos(2\omega t - 2\phi - \epsilon)]$$

Thus the gain ratio affects only the amplitude of the product. Examining the term in brackets, we observe that the product is an oscillation at twice the input frequency with an amplitude of 1, offset from zero by  $\cos \epsilon$  in the positive direction. For no phase error,  $\epsilon = 0$ , the product varies from zero to +2. For  $\epsilon = \pm 30^\circ$ ,  $\cos \epsilon = 0.87$ , and the product varies from -0.13 to +1.87; i.e., there is only about 6 per cent negative overshoot.

*SV waves.* In this case, the earth motion may be given by

$$L = L_0 \cos \omega t \quad Z = -Z_0 \cos \omega t$$

Using the same instrumental constants as for the  $P$  waves, we get, for the product,

$$L'G' = \frac{\beta G^2 L_0 Z_0}{2} [-\cos \epsilon - \cos(2\omega t - 2\phi - \epsilon)]$$

In this case, for the bracketed term, the product is an oscillation at twice the input frequency, and it has an amplitude of 1, offset from zero by  $\cos \epsilon$  in the negative direction. For no phase error,  $\epsilon = 0$ , the product varies from zero to -2, and for an error,  $\epsilon = \pm 30^\circ$ , the product varies from +0.13 to -1.87, representing a positive overshoot of about 6 per cent.

*Rayleigh waves.* In this case, the earth motion may be given by

$$L = L_0 \cos \omega t \quad Z = Z_0 \sin \omega t$$

The instrument outputs become

$$L' = GL_0 \cos(\omega t - \phi)$$

$$Z' = \beta GZ_0 \sin(\omega t - \phi - \epsilon)$$

and we get, for the product,

$$L'Z' = \beta G^2 L_0 Z_0 \cos(\omega t - \phi) \sin(\omega t - \phi - \epsilon)$$

or

$$L'Z' = \frac{\beta G^2 L_0 Z_0}{2}$$

$$\cdot [-\sin \epsilon + \sin (2\omega t - 2\phi - \epsilon)]$$

Again we see that the gain ratio affects only the amplitude of the product. For zero phase error,  $\epsilon = 0$ , if we consider only the bracketed term, the output oscillates symmetrically about zero with a peak-to-peak amplitude of 2 at twice the input frequency. For a phase error,  $\epsilon = +30^\circ$ ,  $-\sin \epsilon = -1/2$ , and the output varies from  $-3/2$  to  $+1/2$ ; i.e., the output is 75 per cent below the zero line. For a negative phase error,  $\epsilon = -30^\circ$ , the output is 75 per cent above the zero line. For prograde elliptical particle motion, the effects of phase error would be reversed. An error of  $\epsilon = 6^\circ$  would produce about 10 per cent asymmetry in the record of a pure Rayleigh wave.

Differences in magnification do not affect phase separation obtained by taking the  $LZ$  product, but differences in phase response do. Fairly large phase errors do not seriously affect the results for rectilinear particle motion but tend to make elliptical motion look like  $P$  or  $SV$ .

Errors in azimuth caused either by an error in epicenter location or by deviation of the waves from the great-circle path produce 'cross-talk' on the records of  $L$  and  $T$ . For incident  $P$  and  $SV$  waves,

$$L_0/L = \cos \delta \quad T_0/L = \sin \delta$$

where  $L_0$  and  $T_0$  are the observed signals on the  $L$  and  $T$  outputs,  $L$  is the actual longitudinal horizontal motion, and  $\delta$  is the angular difference between the actual and assumed direction of propagation. Similarly, for incident  $SH$  waves,

$$T_0/T = \cos \delta \quad L_0/T = \sin \delta$$

where  $T$  is the actual transverse horizontal motion.

When longitudinal and transverse horizontal components are obtained from original N-S and E-W records, both amplitude and phase errors can affect the results. Consider the horizontal component of an incident longitudinal wave,  $L$ , at azimuth  $\theta$ . The ground motion is

$$L = L_0 \cos \omega t$$

or

$$N = L_0 \cos \theta \cos \omega t$$

$$E = L_0 \sin \theta \cos \omega t$$

The horizontal seismometer output may be written

$$N' = GL_0 \cos \theta \cos (\omega t - \phi)$$

$$E' = \beta GL_0 \sin \theta \cos (\omega t - \phi - \epsilon)$$

where  $G$  and  $\phi$  are the amplitude and phase response of the N-S instrument and  $\beta$  and  $\epsilon$  are the gain ratio and phase lag between the N-S and E-W outputs.

The longitudinal output is

$$L' = N' \cos \theta + E' \sin \theta$$

$$= GL_0 [\cos^2 \theta \cos (\omega t - \phi) + \beta \sin^2 \theta \cos (\omega t - \phi - \epsilon)]$$

$$L' = GL_0 \{ [\cos^2 \theta + \beta \cos \epsilon \sin^2 \theta] \cdot \cos (\omega t - \phi) + \beta \sin \epsilon \sin^2 \theta \sin (\omega t - \phi) \}$$

The magnitude of  $L'$ , then, is

$$|L'| = GL_0 [\cos^4 \theta + 2\beta \cos \epsilon \sin^2 \theta \cdot \cos^2 \theta + \beta^2 \sin^4 \theta]^{1/2}$$

Since it is reasonable to consider  $\epsilon$  small,

$$|L'| \simeq GL_0 (\beta \sin^2 \theta + \cos^2 \theta)$$

The phase error,  $\lambda$ , is given by

$$\tan \lambda = \beta \sin \epsilon \sin^2 \theta / (\cos^2 \theta + \beta \cos \epsilon \sin^2 \theta)$$

and

$$\tan \lambda \simeq \lambda \simeq \epsilon \beta \tan^2 \theta / (1 + \beta \tan^2 \theta) \leq \epsilon$$

The transverse output is

$$\begin{aligned} T' &= N' \sin \theta - E' \cos \theta \\ &= GL_0 \sin \theta \cos \theta [\cos (\omega t - \phi) - \beta \cos (\omega t - \phi - \epsilon)] \end{aligned}$$

$$\begin{aligned} T' &= \frac{GL_0}{2} \sin 2\theta [(1 - \beta \cos \epsilon) \cos (\omega t - \phi) \\ &\quad - \beta \sin \epsilon \sin (\omega t - \phi)] \end{aligned}$$

The magnitude of  $T'$  is

$$|T'| = \frac{GL_0}{2} \sin 2\theta [\beta^2 - 2\beta \cos \epsilon + 1]^{1/2}$$

For  $\epsilon$  small, the observed transverse component becomes

$$|T'| \simeq \frac{GL_0}{2} \sin 2\theta(1 - \beta)$$

The ratio of the magnitudes of the observed transverse and longitudinal components, for  $\epsilon$  small, is

$$\begin{aligned} |T'|/|L'| &= (1 - \beta) \sin 2\theta / 2(\beta \sin^2 \theta + \cos^2 \theta) \\ &= (1 - \beta) \tan \theta / (\beta \tan^2 \theta + 1) \end{aligned}$$

The maximum ratio occurs for  $\tan^2 \theta = 1/\beta$  where

$$|T'|/|L'| = (1 - \beta)/2\beta^{1/2}$$

and, for  $\beta \approx 1$ ,

$$|T'|/|L'| \simeq (1 - \beta)/2, \quad \theta = \pi/4$$

Summarizing these results, we can say (1) to the first order, a small error in phase does not affect the separation of  $L$  and  $T$ ; (2) an amplitude error produces apparent  $T$  from incident  $L$  proportionately to the amount of error,  $(1 - \beta)$ , the ratio of  $T'$  to  $L'$  being less than the error; and (3) the resulting phase error in observed  $L$  is equal to or less than the greatest individual phase error.

Analogous results would be obtained from an analysis of incident  $SH$  motion.

**Acknowledgments.** The research reported herein was supported by the National Aeronautics and Space Administration, under contract NASw-82, and by the Air Force Cambridge Research Center under contracts AF19(604)8485 and AF19(604)7376, as part of project Vela, sponsored by the Advanced Research Projects Agency, Department of Defense.

We gratefully acknowledge the assistance of T. Potter and S. Eittreim on this project during the summer of 1962.

#### REFERENCES

- Benioff, H., and B. Gutenberg, Progress report, Seismological Laboratory, California Institute of Technology, for 1951, *Trans. Am. Geophys. Union*, **33**, 759-762, 1952.
- Bogert, B., The transfer function of a short-period vertical seismograph, *Bull. Seismol. Soc. Am.*, **51**, 503-514, 1961a.
- Bogert, B., Seismic data collection, reduction and digitization, *Bull. Seismol. Soc. Am.*, **51**, 515-525, 1961b.
- Cook, K., S. Algermissen, and J. Costain, The status of  $PS$  converted waves in crustal studies, *J. Geophys. Res.*, **67**, 4769-4778, 1962.
- Cooper, G., and P. Broom, Fourier analysis on analog computers (extract), *Instr. Control Systems*, **35**, 155-160, 1962.
- De Bremaecker, J., P. Donoho, and J. Michel, A direct digitizing seismograph, *Bull. Seismol. Soc. Am.*, **52**, 661-672, 1962.
- Espinosa, A., G. Sutton, and H. Miller, A transient technique for seismograph calibration, *Bull. Seismol. Soc. Am.*, **52**, 767-779, 1962.
- Ewing, M., S. Mueller, M. Landisman, and Y. Satô, Transient analysis of earthquake and explosion arrivals, *Geofis. Pura Appl.*, **44**, 83-118, 1959.
- Ewing, M., S. Mueller, M. Landisman, and Y. Satô, Transient phenomena in explosive sound, *Proc. Intern. Congr. Acoustics*, 3rd, edited by L. Cremer, pp. 274-276, Elsevier Publishing Co., Amsterdam, 1961a.
- Ewing, M., S. Mueller, M. Landisman, and Y. Satô, Dispersive transients in earthquake signals, *Proc. Intern. Congr. Acoustics*, 3rd, edited by L. Cremer, pp. 426-428, Elsevier Publishing Co., Amsterdam, 1961b.
- Hagelbarger, D., A digitally encoded seismometer (abstract), *Earthquake Notes*, **32**, 21, 1961.
- Haskell, N. Crustal reflection of plane  $P$  and  $SV$  waves, *J. Geophys. Res.*, **67**, 4751-4767, 1962.
- Haubrich, R., and H. Iyer, Digital seismograph system for measuring earth noise, *Bull. Seismol. Soc. Am.*, **52**, 87-93, 1962.
- Landisman, M., Y. Satô, and M. Ewing, The distortion of pulse-like earthquake signals by seismographs, *Geophys. J.*, **2**, 101-115, 1959.
- Miller, W., The Caltech digital seismograph, *J. Geophys. Res.*, **68**, 841-847, 1963.
- Newstead, G., and P. Watt, A telemetered seismic net in Tasmania, *Nature*, **186**, 704-705, 1960.
- Omote, S., S. Miyamura, and Y. Yamazaki, Triggered magnetic tape recorder for routine seismic observations, *Bull. Earthquake Res. Inst.*, **33**, 397-409, 1955.
- Omote, S., and Y. Yamazaki, Seven channel triggered magnetic tape recorder for routine seismic observations, *Bull. Earthquake Res. Inst.*, **35**, 595-612, 1957.
- Page, R., and J. Oliver, Concurrent storms of long and ultra-long period microseisms, *Bull. Seismol. Soc. Am.*, **53**, 15-26, 1963.
- Pomeroy, P., Seismic waves from large, near-surface nuclear explosions, *Bull. Seismol. Soc. Am.*, **53**, 109-150, 1963.
- Sharpe, J., Motion of the surface of the earth in the compressional phase of a deep-focus earthquake, *Bull. Seismol. Soc. Am.*, **25**, 199-222, 1935.
- Simpson, S., Initial studies on underground nuclear detection with seismic data prepared by a novel digitizing system, *Ann. Rept. 1, Air Force Contract AF19(604)7378*, 1961.
- Willmore, P., The detection of earth movements, in *Methods and Techniques in Geophysics*, 1, edited by S. Runcorn, pp. 230-276, Interscience Publishers, New York, 1960.